Generation and Manipulation of Optical Ferris Wheel by Nested Spiral-Array Plates

Wenren Li, Pusheng Liu, Chaobin Lu, Fengjiang Peng, Heng Gao, and Yuanjie Yang

***Abstract*—Orbital angular momentum of light has attracted great attention in recent years. Optical ferris wheel, composed of the superposition of different orbital-angular-momentum modes, further broadens the application of orbital angular momentum of light in many fields. Here, we experimentally demonstrate a simple way to produce optical ferris wheel with controllable orbital-angular-momentum modes using a mask of spiral arrays. We show that optical ferris wheel can be rotated by adjusting the spiral arrays, and the rotation angle is studied analytically and experimentally. Our technique shows the advantages of wide operation bandwidth and flexible manipulation and the simplicity of our method may find potential application in optical manipulation.**

***Index Terms*—Optical ferris wheel, orbital angular momentum, spiral arrays.**

I. Introduction

OPTICAL vortex with a phase factor $\exp(il\varphi)$ carries well-defined orbital angular momentum (OAM), exhibiting central null intensity and helical wavefront, where l and φ are topological charge and azimuthal angle in the cylindrical coordinate system, respectively [1]. Optical vortex is of particular interest due to its unique characteristics, and it is potential for various applications such as micromanipulations [2], [3], optical pump [4], optical communications [5], [6], detection [7], etc. To enable rising applications, several methods have been proposed for the generation of an optical vortex, ranging from spiral phase plates [8], computer-generated holograms [9], q-plates [10], metasurface [11]–[14], phase retrieval method [15], to cone lens [16].

Recently, the superposition of optical vortices with different OAM modes, i.e., optical ferris wheel (OFW), have attracted appreciable interest [17]–[19] due to its wide applications [20], [21]. Compared with the regular OAM beams, although the OFW loses the helical phase structure, it forms a uniform ring well, which provides a solution for trapping ultralcold atoms [21] and realizing collisional quantum gates [22]. Paterson *et al.* demonstrated that OFW could be used to trapped microscopic particles [20]. Lavery and his collaborators successfully used OFW to detect the angular velocity of rotating objects based on the rotational Doppler effect [7]. Zhang *et al.* successfully used OFW to measure polarization states of light [23]. Furthermore, Lembessis *et al.* demonstrate that OFW can be used for the realization of scalable quantum computation [22]. Besides classical methods, based on pinhole plates [24] or diffractive gratings [25], the recent introduction of alternative methods, namely, photon sieves [26]–[28], spiral zone phase [29] pave the way towards the generation of OFW. However, the OFW generated by above mentioned methods contain fixed OAM modes, and few studies have been done on how to simply control the rotation or the rotational properties of OFW.

In this study, we propose a technique based on structured spiral arrays for generating OFW with controllable OAM modes. We first show such structures and then experimentally demonstrate the effectiveness of our method. In addition, we show that the OAM modes of the generated OFW can be controlled by propagation distance. Furthermore, we demonstrate that the OFW can be rotated by introducing the relative rotation between two spiral arrays. Benefiting from the simplicity of our technique, these structures are promising and competitive in many applications, such as optical tweezers and ultracold atoms.

II. Methods

Several identical spirals uniformly distributed along the azimuthal direction are regarded as basic unit of our structures. As shown in Fig. 1(a), it illustrates that 4 identically clockwise spirals are uniformly arranged along the azimuthal direction. Each spiral consists of a number of pinholes located at a special position and the radius and azimuthal angle of the *n*th pinhole of the spiral, measured from the center, can be expressed as $r_n = ({r_0}^2 + l_a z_0 \lambda \alpha_n/\pi)^{1/2}$ and $\alpha_n = 2\pi n/M$ [30]–[32]. Here, l_a is parameter concerning local topological charges [31], z_0 is the distance of observation plane, M, r_0 and λ denote the number of pinholes, the initial radius and the wavelength, respectively.

The field of a plane wave diffracted by a mask with a transmittance function $\mathrm{T}(x_0, y_0)$ can be written as:

$$u\ (x,y,z) = \frac{\exp\left(\mathrm{ikz}\right)}{i\lambda z} \iint_{-\infty}^{+\infty} T\left(x_0, y_0\right) \exp\left\{\frac{ik}{2z}\left[\left(x-x_0\right)^2 + \left(y-y_0\right)^2\right]\right\} dx_0 dy_0 \tag{1}$$

where λ is wavelength, k is wave number.

Manuscript received April 13, 2022; revised May 19, 2022; accepted May 23, 2022. Date of publication May 26, 2022; date of current version June 9, 2022. This work was supported by the National Natural Science Foundation of China under Grants 11874102 and 12174047. *(Corresponding authors: Pusheng Liu; Yuanjie Yang.)*

The authors are with the University of Electronic Science and Technology of China, Chengdu 611731, China (e-mail: 201921120113@std.uestc.edu.cn; psliu@uestc.edu.cn; 202021120113@std.uestc.edu.cn; 202022120316@std.uestc.edu.cn; 202022120328@std.uestc.edu.cn; dr.yang2003@uestc.edu.cn).

Digital Object Identifier 10.1109/JPHOT.2022.3178079

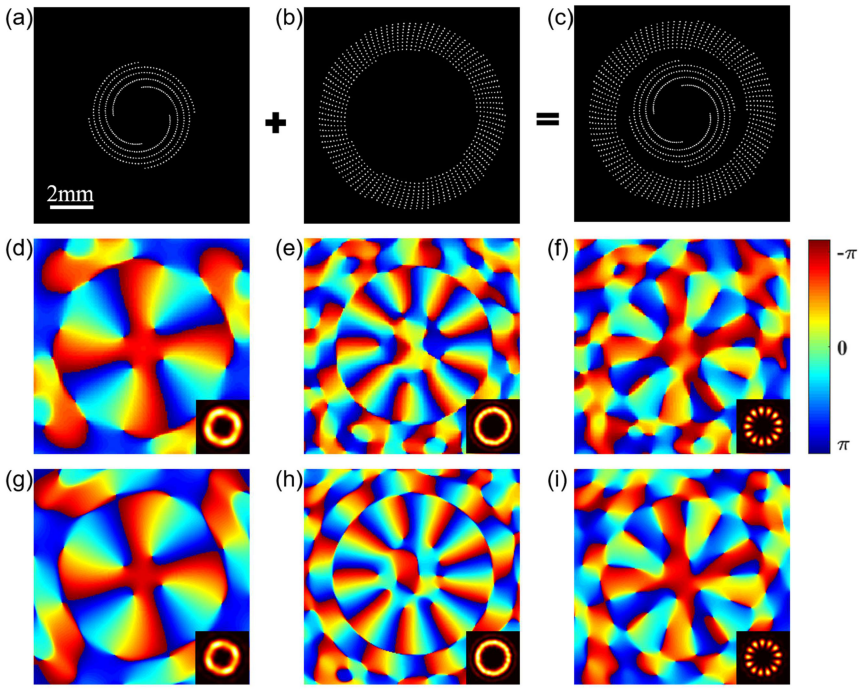

Fig. 1. Schematic plot for generating OFW. (a) and (b) Two masks with 4 clockwise spirals and 9 counterclockwise spirals; (c) The nested mask with (a) and (b); (d)–(f) and (g)–(i) The corresponding phase distribution of the diffracted field illuminated with a plane wave of wavelength $\lambda = 632.8$ nm and $\lambda = 532.8$ nm, respectively. The inserted patterns in (d)–(i) are the corresponding intensity patterns.

According to Eq. (1), the phase distribution and intensity patterns of diffractive field generated by the mask (Fig. 1(a)) are shown in Fig. 1(d) under the illumination of a plane wave of wavelength $\lambda = 632.8$ nm. We can see that an optical vortex with OAM mode $l = -4$ can be generated with this rotationally symmetric spiral structures, which can be explained by theory of mode selection [30]. The theory states that this *m*-order rotationally symmetric structure composed of several spirals can select the OAM modes that are multiples of *m* and focus an OAM mode we want near the optical axis by adjusting spirals [24].

Another mask including 9 counterclockwise spirals is given in Fig. 1(b). An optical vortex with OAM mode $l = 9$ and corresponding phase distribution are shown in Fig. 1(e). In addition, it is worth noting that the signs of the OAM modes indices in Fig. 1(d) and (e) are determined by the handedness (clockwise or counterclockwise) of spirals [24].

It is noted that the superposition of two optical vortices with different OAM modes generate an intensity distribution consisting of several petal-like structures, i.e., OFW. In order to generate OFW, structures in Fig. 1(a) and (b) are nested together to construct nested spiral-array plate (NSP), as shown in Fig. 1(c). Under the illumination of a plane wave, the intensity distribution after this NSP should be the interference of two aforementioned fields. Accordingly, OFW with 13 bright petals can be generated by mask Fig. 1(c). The corresponding phase distribution and intensity patterns are given in Fig. 1(f). OFW with OAM modes of $l_1 = -4$ and $l_2 = 9$ (corresponding to the inner and outer spiral arrays, respectively) further prove the effectiveness of our method. Fig. 1(g), (h) and (i) show the corresponding simulation results obtained by illuminating the above masks with a plane wave with a wavelength of $\lambda = 532.8$ nm. From Fig. 1, we can see that our mask can work for different wavelength.

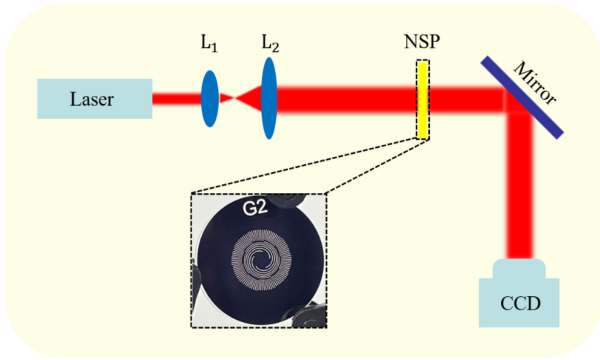

Fig. 2. Experimental setup for generating OFW; CCD: Charge-coupled device; L_1, L_2: A pair of lens; NSP: Nested spiral-array plate we designed; A sample of physical NSP we produced with a mark "G2".

III. Results and Discussion

A. Generation of OFW

Fig. 2 shows the experimental setup for producing OFW. A beam is expended and collimated by a pair of lens (L_1, L_2), and then passes through the NSP we designed. At a given propagation distance, the intensity patterns generated by OFW are captured by charge-coupled device (CCD). The NSP for our experiment was produced from a circular SiO_2 substrate (2 cm in diameter) plated with Cr film, and the diameter of each pinhole

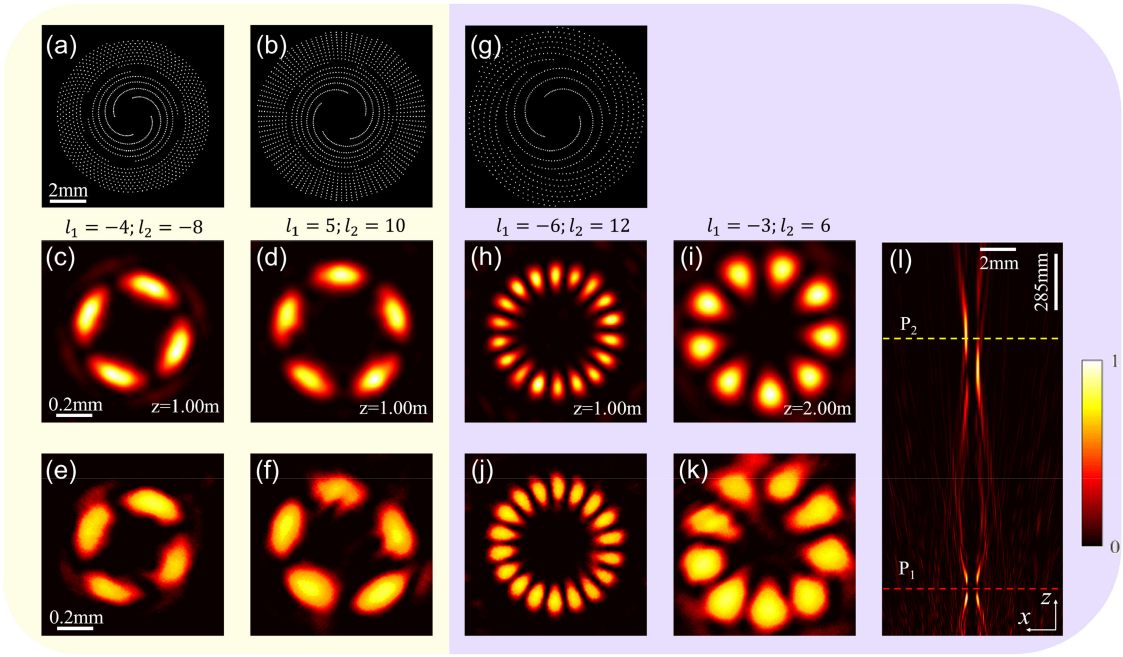

Fig. 3. Generation of OFW through different NSPs. (a), (b) and (g) Represent NSPs we designed; The simulation results of intensity distribution at a given plane are given in (c), (d), (h) and (i); (e), (f), (j) and (k) are the corresponding experimental results, respectively; (l) Shows the intensity distribution of light field generated by mask (g) in the *x*-*z* plane.

is 30 μm. Due to the diffraction effect, the energy utilization rate is relatively low.

Using the aforementioned method, we give some examples of producing OFW in Fig. 3. Fig. 3(a) and (b) are the NSPs we designed (4 clockwise spirals and 8 clockwise spirals in NSP (a), 5 counterclockwise spirals and 10 counterclockwise spirals in NSP (b)). In the experiment, we choose a laser with a wavelength of 632.8 nm. Fig. 3(c) and (d) are the corresponding simulation results at given propagation distance $z = 1.00$ m, which are several different petal-like patterns. At the same time, the experimental results are also given in Fig. 3(e) and (f), which are in good agreement with the simulation results and illustrate the effectiveness and correctness of our technique.

Compared with our previous work [24], this method of nested spiral arrays with different initial radii can generate superposition OAM more flexibly, rather than simply adding two OAM modes with opposite topological values $\pm l$.

Moreover, it is known that the local topological charges of the optical field generated by this spiral structure are inversely proportional to the propagation distance [31]. According to this principle, we design a special NSP that the OAM modes of OFW generated by it will change with the propagation distance. That is to say, the OFW with variable intensity patterns can be obtained by our proposed NSP. Unlike traditional OFW, the number of petals of OFW generated by our method will decrease along the propagation axis in free space. Fig. 3(g) shows the NSP containing 3 clockwise spirals inner part and 6 counterclockwise spirals outer part, and the local topological charges of inner (outer) spirals change from $l_1 = -6$ ($l_2 = 12$) at propagation distance $z = 1.00$ m to $l_1 = -3$ ($l_2 = 6$) at propagation distance $z = 2.00$ m.

Simulation results (Fig. 3(h)) exhibit the intensity pattern of 18 bright petals at $z = 1.00$ m. Interesting, as illustrated in Fig. 3(i), we can see that OFW with 9 petals are observed in the plane $z = 2.00$ m. Fig. 3(j) and (k) are the corresponding experimental results, which agree well with simulation results. Therefore, one can note that the number of petals in OFW decrease with the increase of the propagation distance, which may provide another scheme in three-dimensional particle manipulation. It is clearly that the change in the OAM modes of the OFW generated by the NSP shown in Fig. 3(g) is inversely proportional to the propagation distance, which at the same time does not violate the theory of mode selection theory (OAM modes is also an integral multiple of the number of spirals).

Fig. 3(l) shows the simulation results of the intensity distribution of the transmitted light generated by mask (g) in the *x*-*z* plane. It can be seen from the figure that the light field modulated by the mask is focused twice in the propagation direction. The OAM modes of $l_1 = -6$ and $l_2 = 12$ are focused near the optical axis at the plane P_1 ($z = 1.00$ m), and the intensity distribution of this plane corresponds to Fig. 3(h). When the receiving screen is moved to a distance of $z = 2.00$ m from the mask (P_2 in Fig. 3(l)), the other two OAM modes ($l_1 = -3$ and $l_2 = 6$) are focused near the optical axis, and the intensity distribution at this plane is shown in Fig. 3(i).

Unlike conventional optical vortex with a single OAM mode, the optical ferris wheel forms a ring-shaped potential well in the angular direction, which can be used to control colloidal rings [33] or ultracold atoms [21]. In addition, optical ferris wheel has also been shown to be useful for ultrasensitive angular measurement using OAM entanglement between photon-pairs in

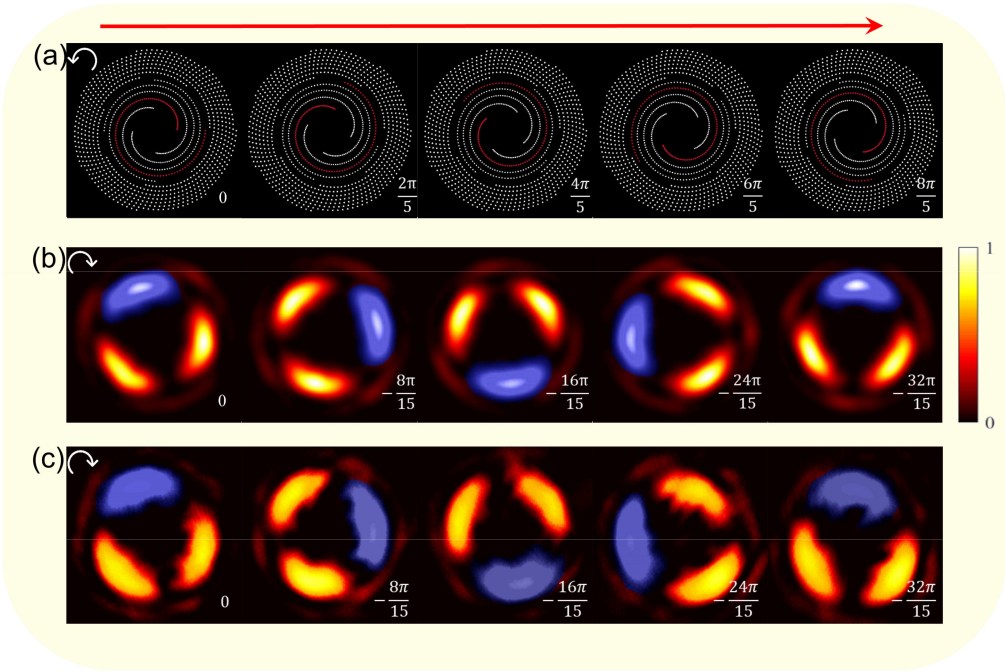

Fig. 4. The rotation of the OFW. (a) NSPs with rotating inner spirals; (b) Simulation results of intensity patterns; (c) The corresponding experimental results. In order to observe the rotational angle, a spiral arm of each NSP is marked red and a petal of the OFW is marked in blue. The white rotating arrows indicate the rotational direction of the spiral arrays. The number below each picture represents the rotational angle of the inner spiral arrays relative to the original one.

Spontaneous Parametric Down Conversion [34] and generating superpositions of atomic rotational states based on the coherent transfer of the OAM of a photon to an atom [35].

B. The Influences of Rotating Spiral Arrays on the OFW

Since OFW have application prospects in many fields, it has attracted significant attention [22], [36]. In particle manipulation, we often need a rotational OFW to control particles dynamically. Usually, the rotation of OFW can be achieved by introducing frequency shift [21] and phase shift [20].

Here, we show how to rotate the OFW by tuning the structure of NSP. We can achieve the rotation of the OFW by introducing relative rotation between the inner and outer spiral arrays. As shown in Fig. 4(a), these NSPs are composed of 4 counterclockwise spirals inner part and 7 counterclockwise spirals outer part ($l_1 = 4$ and $l_2 = 7$), and the inner spiral arrays of each NSP rotate $2\pi/5$ counterclockwise in sequence. Under the illumination of a plane wave, the corresponding simulation and experimental results are listed in Fig. 4(b) and (c), respectively. Surprisingly, it can be observed that the OFW rotate $8\pi/15$ clockwise under the case of the inner spiral array rotating $2\pi/5$ counterclockwise each time.

Now let us explain why this is the case. Without loss of generality, the complex optical fields generated by inner and outer spiral arrays can be expressed as $E_1\ (r,\varphi) = A(r)\exp(il_1\varphi)$ and $E_2\ (r,\varphi) = A(r)\exp(il_2\varphi)$, respectively. If the inner spiral array is rotated by an angle of $\Delta\varphi_1$ in the counterclockwise direction, and then the complex field generated inner spiral array becomes $E_1'\ (r,\varphi) = A(r)\exp[il_1(\varphi - \Delta\varphi_1)]$. Therefore, the intensity patterns of superimposed field can be written as

$$\mathrm{I} = |E_1' + E_2|^2 = 4|A\,(r)|^2\cos^2\left[\frac{(l_1 - l_2)\,\varphi - l_1\Delta\varphi_1}{2}\right] \tag{2}$$

We can easily get the rotational angle of OFW as

$$\Delta\varphi = \frac{l_1}{l_1 - l_2}\,\Delta\varphi_1 \tag{3}$$

From (3), we can clearly see that the rotational angle $\Delta\varphi$ is different from that of the inner spiral array, owing to the fact that $\Delta\varphi$ is determined not only by $\Delta\varphi_1$, but also l_1 and l_2. Therefore, we can understand the rotation angle in Fig. 4 clearly using (3). Moreover, the rotational direction of the OFW is opposite to that of the spiral array due to the negative value of $l_1/(l_1 - l_2)$.

IV. Conclusion

In summary, we proposed a simple way to generate OFW based on two spiral arrays and the OFW can be rotated by introducing relative rotation between the two spiral arrays. This technique provides a feasible scheme for the generation and manipulation of OFW, which can broaden the application of OAM of light. In addition, the pattern of our generated OFW varies with propagation distance, which provides a solution for three-dimensional trapped structures [37]. The tunable rotation of the OFW achieved by our method may provide an efficient scheme for the dynamic control of particles in optical tweezers.

REFERENCES

[1] L. Allen, M. W. Beijersbergen, R. J. C. Spreeuw, and J. P. Woerdman, "Orbital angular momentum of light and the transformation of Laguerre-Gaussian laser modes," *Phys. Rev. A*, vol. 45, no. 11, pp. 8185–8189, Jun. 1992, doi: 10.1103/PhysRevA.45.8185.

[2] G. Rui, X. Wang, and Y. Cui, "Manipulation of metallic nanoparticle with evanescent vortex Bessel beam," *Opt. Exp.*, vol. 23, no. 20, pp. 25707–25716, Sep. 2015, doi: 10.1364/OE.23.025707.

[3] M. Gecevicius, R. Drevinskas, M. Beresna, and P. G. Kazansky, "Single beam optical vortex tweezers with tunable orbital angular momentum," *Appl. Phys. Lett.*, vol. 104, Jun. 2014, Art. no. 231110, doi: 10.1063/1.4882418.

[4] J. Leach, H. Mushfique, R. di Leonardo, M. Padgett, and J. Cooper, "An optically driven pump for microfluidics," *Lab Chip*, vol. 6, pp. 735–739, Apr. 2006, doi: 10.1039/B601886F.

[5] J. Wang *et al.*, "Terabit free-space data transmission employing orbital angular momentum multiplexing," *Nature Photon.*, vol. 6, pp. 488–496, Jun. 2012, doi: 10.1038/nphoton.2012.138.

[6] L. Liu, Y. Gao, and X. Liu, "High-dimensional vortex beam encoding/decoding for high-speed free-space optical communication," *Opt. Commun.*, vol. 452, pp. 40–47, Dec. 2019, doi: 10.1016/j.optcom.2019.06.061.

[7] M. P. J. Lavery, F. C. Speirits, S. M. Barnett, and M. J. Padgett, "Detection of a spinning object using light's orbital angular momentum," *Science*, vol. 341, no. 6145, pp. 537–540, Aug. 2013, doi: 10.1126/science.1239936.

[8] M. W. Beijersbergen, R. P. C. Coerwinkel, M. Kristensen, and J. P. Woerdman, "Helical-wavefront laser beams produced with a spiral phaseplate," *Opt. Commun.*, vol. 112, pp. 321–327, Dec. 1994, doi: 10.1016/0030-4018(94)90638-6.

[9] N. R. Heckenberg, R. McDuff, C. P. Smith, and A. G. White, "Generation of optical phase singularities by computer-generated holograms," *Opt. Lett.*, vol. 17, no. 3, pp. 221–223, Feb. 1992, doi: 10.1364/OL.17.000221.

[10] L. Marrucci, C. Manzo, and D. Paparo, "Optical spin-to-orbital angular momentum conversion in inhomogeneous anisotropic media," *Phys. Rev. Lett.*, vol. 96, no. 16, Apr. 2006, Art. no. 163905, doi: 10.1103/PhysRevLett.96.163905.

[11] Q. Zheng *et al.*, "Efficient orbital angular momentum vortex beam generation by generalized coding metasurface," *Appl. Phys. A*, vol. 125, Jan. 2019, Art. no. 136, doi: 10.1007/s00339-018-2373-z.

[12] Z. Zhao, J. Wang, S. H. Li, and A. E. Willner, "Metamaterials-based broadband generation of orbital angular momentum carrying vector beams," *Opt. Lett.*, vol. 38, no. 6, pp. 932–934, Mar. 2013, doi: 10.1364/OL.38.000932.

[13] N. Yu *et al.*, "Light propagation with phase discontinuities: Generalized laws of reflection and refraction," *Science*, vol. 334, no. 6054, pp. 333–337, Oct. 2011, doi: 10.1126/science.1210713.

[14] X. Liu, J. Deng, M. Jin, Y. Tang, and G. Li, "Cassegrain metasurface for generation of orbital angular momentum of light," *Appl. Phys. Lett.*, vol. 115, Nov. 2019, Art. no. 221102, doi: 10.1063/1.5127007.

[15] Z. Liu et al*et al.*, "Generation of hollow beam by using phase filtering with multi-distance phase retrieval," *Opt. Commun.*, vol. 456, Feb. 2020, Art. no. 124611, doi: 10.1016/j.optcom.2019.124611.

[16] M. Mansuripur, A. R. Zakharian, and E. M. Wright, "Spin and orbital angular momenta of light reflected from a cone," *Phys. Rev. A*, vol. 84, no. 3, Sep. 2011, Art. no. 033813, doi: 10.1103/PhysRevA.84.033813.

[17] R. Mamuti, S. Goto, K. Miyamoto, and T. Omatsu, "Generation of coupled orbital angular momentum modes from an optical vortex parametric laser source," *Opt. Exp.*, vol. 27, no. 25, pp. 37025–37033, Dec. 2019, doi: 10.1364/OE.27.037025.

[18] S. Vyas, Y. Kozawa, and S. Sato, "Polarization singularities in superposition of vector beams," *Opt. Exp.*, vol. 21, no. 7, pp. 8972–8986, Apr. 2013, doi: 10.1364/OE.21.008972.

[19] B. P. da Silva, D. S. Tasca, E. F. Galvão, and A. Z. Khoury, "Astigmatic tomography of orbital-angular-momentum superpositions," *Phys. Rev. A*, vol. 99, no. 4, Apr. 2019, Art. no. 043820, doi: 10.1103/PhysRevA.99.043820.

[20] L. Paterson, M. P. MacDonald, J. Arlt, W. Sibbett, P. E. Bryant, and K. Dholakia, "Controlled rotation of optically trapped microscopic particles," *Science*, vol. 292, no. 5518, pp. 912–914, May. 2001, doi: 10.1126/science.1058591.

[21] S. Franke-Arnold *et al.*, "Optical ferris wheel for ultracold atoms," *Opt. Exp.*, vol. 15, no. 14, pp. 8619–8625, Jun. 2007, doi: 10.1364/OE.15.008619.

[22] V. E. Lembessis, A. Lyras, and O. M. Aldossary, "Optical Ferris wheels as a platform for collisional quantum gates," *J. Opt. Soc. Amer. B*, vol. 38, no. 1, pp. 233–240, Jan. 2021, doi: 10.1364/JOSAB.405193.

[23] Z. Zhang, J. Han, D. Geng, Y. Wang, and A. Ma, "Superposition of optical vortex beams for polarization measurement," *IEEE Photon. J.*, vol. 13, no. 6, Dec. 2021, Art no. 6500106, doi: 10.1109/JPHOT.2021.3117952.

[24] Y. Yang, Q. Zhao, L. Liu, Y. Liu, C. Rosales-Guzmán, and C.-W. Qiu, "Manipulation of orbital-angular-momentum spectrum using pinhole plates," *Phys. Rev. Appl.*, vol. 12, no. 6, Dec. 2019, Art. no. 064007, doi: 10.1103/PhysRevApplied.12.064007.

[25] J. C. T. Lee, S. J. Alexander, S. D. Kevan, S. Roy, and B. J. McMorran, "Laguerre–Gauss and Hermite–Gauss soft X-ray states generated using diffractive optics," *Nature Photon.*, vol. 13, pp. 205–209, Jan. 2019, doi: 10.1038/s41566-018-0328-8.

[26] R. Liu, F. Li, M. J. Padgett, and D. B. Phillips, "Generalized photon sieves: Fine control of complex fields with simple pinhole arrays," *Optica*, vol. 2, no. 12, pp. 1028–1036, Dec. 2015, doi: 10.1364/OPTICA.2.001028.

[27] Z. Jin *et al.*, "Phyllotaxis-inspired nanosieves with multiplexed orbital angular momentum," *eLight*, vol. 1, Sep. 2021, Art. no. 5, doi: 10.1186/s43593-021-00005-9.

[28] Y. Bai, H. Lv, X. Fu, and Y. Yang, "Vortex beam: Generation and detection of orbital angular momentum," *Chin. Opt. Lett.*, vol. 20, no. 1, Jan. 2022, Art. no. 012601, doi: 10.3788/COL202220.012601.

[29] Y. Lan, Y. Qian, and Z. Ren, "Tunable polycyclic chiral beams," *Annalen der Physik*, vol. 532, Apr. 2020, Art. no. 1900530, doi: 10.1002/andp.201900530.

[30] Y. Yang, G. Thirunavukkarasu, M. Babiker, and J. Yuan, "Orbital-angular-momentum mode selection by rotationally symmetric superposition of chiral states with application to electron vortex beams," *Phys. Rev. Lett.*, vol. 119, no. 9, Aug. 2017, Art. no. 094802, doi: 10.1103/PhysRevLett.119.094802.

[31] Y. Yang *et al.*, "Anomalous Bessel vortex beam: Modulating orbital angular momentum with propagation," *Nanophotonics*, vol. 7, no. 3, pp. 677–682, Jan. 2018, doi: 10.1515/nanoph-2017-0078.

[32] Z. Li *et al.*, "Generation of high-order optical vortices with asymmetrical pinhole plates under plane wave illumination," *Opt. Exp.*, vol. 21, no. 13, pp. 15755–15764, Jul. 2013, doi: 10.1364/OE.21.015755.

[33] C. H. J. Schmitz, K. Uhrig, J. P. Spatz, and J. E. Curtis, "Tuning the orbital angular momentum in optical vortex beams," *Opt. Exp.*, vol. 14, no. 15, pp. 6604–6612, Jul. 2006, doi: 10.1364/OE.14.006604.

[34] V. D'Ambrosio *et al.*, "Photonic polarization gears for ultra-sensitive angular measurements," *Nature Commun.*, vol. 4, Sep. 2013, Art. no. 2432, doi: 10.1038/ncomms3432.

[35] M. F. Andersen *et al.*, "Quantized rotation of atoms from photons with orbital angular momentum," *Phys. Rev. Lett.*, vol. 97, no. 17, Oct. 2006, Art. no. 170406, doi: 10.1103/PhysRevLett.97.170406.

[36] H. R. Hamedi, V. Kudriasov, N. Jia, J. Qian, and G. Juzeliunas, "Ferris wheel patterning of Rydberg atoms using electromagnetically induced transparency with optical vortex fields," *Opt. Lett.*, vol. 46, no. 17, pp. 4204–4207, Sep. 2021, doi: 10.1364/OL.427000.

[37] M. P. MacDonald, L. Paterson, K. Volke-Sepulveda, J. Arlt, W. Sibbett, and K. Dholakia, "Creation and manipulation of three-dimensional optically trapped structures," *Science*, vol. 296, no. 5570, pp. 1101–1103, May 2002, doi: 10.1126/science.1069571.